Heliyon 9 (2023) e17336

Contents lists available at ScienceDirect

Heliyon

journal homepage: www.cell.com/heliyon

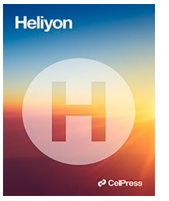

Review article

Cardiac magnetic resonance of hypertrophic heart phenotype: A review

Davide Tore, Riccardo Faletti, Clara Gaetani, Elena Bozzo, Andrea Biondo, Andrea Carisio, Francesca Menchini, Maria Miccolis, Francesco Pio Papa, Martina Trovato, Paolo Fonio, Marco Gatti *

Radiology Unit, Department of Surgical Sciences, AOU Città della Salute e della Scienza di Torino, University of Turin, Turin, Italy

ARTICLE INFO

Keywords:
CMR
HCM
Cardiac hypertrophy
Amyloidosis
Sarcoidosis
Anderson-fabry disease
Iron overload

ABSTRACT

Hypertrophic heart phenotype is characterized by an abnormal left ventricular (LV) thickening. A hypertrophic phenotype can develop as adaptive response in many different conditions such as aortic stenosis, hypertension, athletic training, infiltrative heart muscle diseases, storage disorders and metabolic disorders. Hypertrophic cardiomyopathy (HCM) is the most frequent primary cardiomyopathy (CMP) and a genetical cause of cardiac hypertrophy. It requires the exclusion of any other cause of LV hypertrophy.

Cardiac magnetic resonance (CMR) is a comprehensive imaging technique that allows a detailed evaluation of myocardial diseases. It provides reproducible measurements and myocardial tissue characterization. In clinical practice CMR is increasingly used to confirm the presence of ventricular hypertrophy, to detect the underlying cause of the phenotype and more recently as an efficient prognostic tool.

This article aims to provide a detailed overview of the applications of CMR in the setting of hypertrophic heart phenotype and its role in the diagnostic workflow of such condition.

1. Introduction

The hypertrophic heart phenotype is characterized by an abnormal and mainly asymmetric left ventricular (LV) thickening (at least 15 mm in Caucasian adults, detected in one or more LV myocardial segments) measured by echo-cardiography, MRI, or CT; it is an independent predicting factor for cardiovascular events and sudden cardiac death (SDC), regardless of its cause. A hypertrophic phenotype can develop as adaptive response to allow the normal ejection fraction (EF) despite an increased pressure and/or volume load in many different pathological conditions including aortic stenosis, hypertension, athletic training, infiltrative heart muscle diseases, storage disorders and metabolic disorders. Hypertrophic cardiomyopathy (HCM) represents the most common primary cardiomyopathy (CMP) and a genetical cause of cardiac hypertrophy. It requires the exclusion of any other cause of LV hypertrophy. HCM is the most frequent heritable heart disease and the leading cause of SDC in young people. In such a wide variety of conditions, determine the precise etiology of LV hypertrophy is always a clinical challenge [1,2].

The first-line imaging modality used to investigate LV hypertrophy is echocardiography: it assesses its extension and distribution and evaluates anatomical and functional parameters such as ventricular size, systolic and diastolic function. However, conventional

* Corresponding author.
E-mail address: m.gatti@unito.it (M. Gatti).

https://doi.org/10.1016/j.heliyon.2023.e17336
Received 31 December 2022; Received in revised form 5 June 2023; Accepted 14 June 2023
Available online 19 June 2023

echocardiography is considerably operator-depending, is influenced by acoustic windows, and unable to provide tissue characterization [3].

Cardiac magnetic resonance (CMR) is a comprehensive imaging technique that allows a detailed evaluation of myocardial diseases. It provides both precise and highly reproducible measurements (wall thickness measurements, chamber size, pattern of hypertrophy, and systolic function) and myocardial tissue characterization [3,4]. In clinical practice CMR is increasingly used to confirm the presence of ventricular hypertrophy, to detect the underlying cause of the phenotype and more recently as an efficient prognostic tool, predicting the risk of atrial fibrillation and heart failure, detecting and quantifying fibrosis with late gadolinium enhancement (LGE) evaluation [5,6]. It is also possible to implement tissue characterization by using mapping sequences, which give important information for the diagnosis and prognosis in patients with hypertrophic heart [4].

For the above reasons, CMR is nowadays the best imaging technique to assess myocardial diseases and to define the cause of cardiac hypertrophy. Nevertheless, there are some relative and absolute contraindications to the execution of CMR, such as the presence of pacemaker or implantable cardioverter defibrillator (ICD), the presence of brain clips or incompatible metallic devices, patients that suffer from claustrophobia, or those with cardiac arrhythmias that prevent the required electrocardiogram (ECG) gating. Moreover, CMR has limitations related to resources availability so that the exam is performable only in some centers [7,8]. In this setting, cardiac CT (CCT) has lately emerged as an alternative diagnostic tool to CMR for both fibrosis identification and biventricular function, revealing new indications for a comprehensive assessment of cardiac anatomy, beyond the well-validated and recognized role in the non-invasive study of coronary artery diseases [7,9]. Particularly, CCT provides an accurate measurement of LV wall thickness and biventricular volume and function, matching well with CMR findings [7,9]. CCT provides also myocardial fibrosis assessment, even if with less diagnostic accuracy compared with CMR, due to low contrast-to-noise ratio, and requiring higher doses of contrast agents than CMR. However, recent technology advances appear to make possible myocardial fibrosis assessment using low doses of iodine-based CT contrast agents, particularly with dual-energy CT technology, that simultaneously using different tube potentials provides tissue characterization with ECV evaluation, considered equal to myocardial fibrosis when compared to CMR [7,10]. At present times, the use of CCT to study cardiac diseases is limited to those patients with CMR contraindications or in case of diagnostic doubt, but in the next future there will be probably an increase in clinical application [7,8].

2. CMR protocol

To evaluate patients with suspected LV hypertrophy, cardiac magnetic resonance should be performed on high field scanners, for instance 1.5 T and 3 T; the use of ultra-high field scanners (for example 7 T) is not routinely used in clinical practice, since the technical difficulty to obtain ECG gating and the more frequent presence of artifacts [11,12]. ECG gating and parallel imaging techniques to shorten scans and breath hold times are mandatory [13].

A comprehensive CMR acquisition protocol for the evaluation of cardiac hypertrophic phenotype should encompass of sequences for the evaluation of LV structure and function and other sequences for tissue characterization [2].

The CMR exam starts by acquiring axial, coronal, and sagittal scout images, followed by an axial (8–10 mm slice thickness) series of steady state free precession (SSFP) or single-shot turbo spin echo black-blood morphological images of the chest. Balanced steady-state free precession (bSSFP) technique is the primary method to evaluate the LV; compared to fast gradient echo sequences used in the past, bSSFP technique provides blood-myocardial contrast. Short-axis images (6–8 mm thick with a 2 mm gap between slices) SSFP long-axis pictures collected in 2-chamber, 4-chamber, and 3-chamber (left ventricular outflow tract, LVOT) planes (prescribed from short-axis cine images) provide the necessary data to evaluate LV anatomy and function. Visual analysis of short- and long-axis cine pictures permits qualitative assessment of the existence and distribution of hypertrophy, as well as the size, shape, and function of both ventricles [14].

T2weighted-STIR sequences may be acquired on long-axis two chamber, four chamber and three chamber and on short-axis to evaluate the presence of oedema [15].

CMR myocardial tissue characterization can be quantitatively performed using myocardial parametric imaging with T1 and T2 mapping sequences [16]. Magnetization relaxometry mapping techniques enable the detection of diffuse fibrosis by using native (noncontrast-enhanced) T1 and T2 values, which appears to be robust. In addition, contrast enhanced T1 mapping in conjunction with the hematocrit value is useful for calculating the extracellular volume fraction (ECV), a measure of the proportion of extracellular space within the myocardium that serves as a marker of myocardial remodeling [16]. The modified look locker (MOLLI) and shortened MOLLI (ShMOLLI) sequences are the most frequently employed methods for acquiring T1 mapping values [16,17]. Absolute T1 and T2 values for normal LV myocardium differ among MRI systems and vendors [16]. Numerous studies have demonstrated that some factors can influence the native T1 relaxation time, including the imaging pulse sequence, magnetic field strength (T1 values increase with increasing field strength), acquisition plane (e.g., 2-chamber versus 4-chamber), region of myocardium being sampled, patient's heart rate, age, and sex [18].

The examination is completed after administration of intravenous contrast medium, with the acquisition of inversion recovery (IR) LGE sequences on planes with various orientations [14]. In conventional LGE imaging, the operator manually selects the inversion time (IT) to null the signal of healthy myocardium using a specific sequence (Look Looker, for instance) [19]. To provide the greatest contrast between diseased and normal cardiac tissue, the best IT must be chosen. The advent of phase-sensitive inversion recovery (PSIR) sequences by all vendors has made it easier to obtain correct LGE images and to evaluate the level of cardiac involvement [20].

3. Cardiac mass and volumes: reference ranges

To recognize abnormal conditions, it is essential to know the upper and lower limits of normal and early pathological findings. CMR is extensively used both to determine physiological reference values (including atrial and ventricular function and size, great vessels diameters, flow, and myocardial relaxation times), and to assess the myocardial tissue composition, making it possible to grade disease severity, to evaluate prognosis and to monitor possible changes during therapies [21]. We report normal parameters according to "*Reference ranges ("normal values") for cardiovascular magnetic resonance in adults and children: 2020 update*".

LV diameters are obtained by manual or automatic contouring analysis of the endocardial and epicardial borders on cine bSSFP images, on short-axis view, both in systole and diastole, using a per slice segmentation [21]. Since LV volume and mass are significantly affected by papillary muscles [22–24], they must be included in the segmentation, even if no uniform convention has been accepted to analyze trabeculation and papillary muscle mass. The Society of Cardiovascular Magnetic Resonance (SCMR) recommendations established that papillary muscles should be included either in the LV volume or in the LV mass but not in both [22].

Right ventricle (RV) volume evaluation requires a stack of bSSFP images in the short-axis plane or trans axial plane. RV analysis is performed manually or with semiautomatic software on a per slice basis, by contouring the endocardial border in both systole and diastole. It is very important to include the trabeculations to achieve a higher reproducibility of RV volumes and mass. RV volume reference values have been provided both for papillary muscles included and their exclusion in the segmentation, since the exclusion or the inclusion of papillary muscles has a significant influence on the RV mass and volumes. RV volume depends also on the body surface area (BSA), sex (it is larger in men than in women) and age (there is a decrease with greater age) [21]. Reference values for RV and LV are reported in Table 1 and Table 2. Fig. 1 shows an example of contouring method in our hospital.

Left atrial (LA) volume is usually measured by modified Simpson's method and the biplane area-length method, but also 3-dimensional modelling software has been used [21]. Simpson's method requires a stack of cine bSSFP images either in the short axis, the horizontal long axis or transverse view. The biplane area-length method requires a 2-chamber and a 4-chamber view to measure LA area and its longitudinal and transverse diameter [21], during ventricular systole (the moment in which maximal LA volume is present, usually the last image immediately before opening of the mitral valve). It is important to exclude the LA appendage and pulmonary veins in the segmentation. LA volume is influenced by BSA and gender, but not by age [21].

Regarding right atrium (RA) measurement, the modified Simpson's method, the biplane area-length method and 3D-modeling method have been used to evaluate the RA volumes. Particularly, the biplane area-length method requires a 4-chamber view and a RV 2-chamber view; for Simpson's analysis a stack of cine bSSFP images in the short axis is required. The inferior and superior vena cava are excluded from RA volume. Maximal RA volume is present during ventricular systole (usually the last cine image before the tricuspid valve opens).

Recently, new machine learning systems based on artificial intelligence (AI) have been developed and tested to evaluate heart chambers' volumes, making it possible to obtain results similar to those obtained with manual segmentation in shorter times [25].

4. Hypertrophic cardiomyopathy

HCM is the most common genetic cardiomyopathy. The prevalence of the disease is estimated to be 1:500 to 1:200 [6]. It is caused by one of over 600 mutations, mostly in the sarcomere genes, and transmitted as autosomal dominant trait [6]. Patients can be asymptomatic or present with mild-to-moderate symptoms, but also heart failure or SDC are possible [26]. HCM is the first cause of SDC in young people [6]. The disease can be diagnosed in presence of left ventricular wall thickness >15 mm, not associated with ventricular dilatation, measured in one or more LV myocardial segments by an imaging technique, or a ratio between septal thickness

Table 1
Left ventricular parameters, adapted from "Reference ranges ("normal values") for cardiovascular magnetic resonance in adults and children: 2020 update".

Parameter	Non-athletes [mean ± SD (LL–UL)[c]]		Regular athletes[a] [mean ± SD (LL–UL)[c]]		Elite athletes[b] [mean ± SD (LL–UL)[c]]	
	Men	Women	Men	Women	Men	Women
LVEDV (ml)	201 ± 33 (135–267)	156 ± 22 (112–200)	250 ± 32 (186–314)	194 ± 27 (140–248)	261 ± 39 (183–339)	199 ± 31 (137–261)
LVEDV/BSA (ml/m^2)	101 ± 15 (71–131)	90 ± 11 (68–112)	123 ± 13 (97–149)	107 ± 14 (79–135)	129 ± 17 (95–163)	107 ± 14 (79–135)
LVEDV (ml)	87 ± 19 (49–125)	65 ± 13 (39–91)	108 ± 20 (68–148)	86 ± 15 (56–116)	117 ± 24 (69–165)	85 ± 20 (45–125)
LVEDV/BSA (ml/m^2)	43 ± 10 (23–63)	37 ± 7 (23–51)	53 ± 9 (35–71)	48 ± 8 (32–64)	58 ± 11 (36–80)	46 ± 11 (24–68)
LVM (g)	95 ± 20 (55–135)	60 ± 11 (38–82)	125 ± 22 (81–169)	84 ± 17 (50–118)	139 ± 28 (83–195)	92 ± 15 (62–122)
LVM/BSA (g/m^2)	48 ± 9 (30–66)	34 ± 6 (22–46)	62 ± 11 (40–84)	46 ± 9 (28–64)	69 ± 13 (43–95)	50 ± 8 (34–66)
LVEF (%)	57 ± 6 (45–69)	58 ± 5 (48–68)	57 ± 5 (47–67)	55 ± 4 (47–63)	55 ± 5 (45–65)	58 ± 7 (44–72)
max. IVS (mm)	10 ± 1 (8–12)	5 ± 1 (3–7)	11 ± 1 (9–13)	9 ± 1 (7–11)	11 ± 1 (9–13)	9 ± 1 (7–11)

SD standard deviation, LL lower limit, UL upper limit, n number of study subjects, LV left ventricular, EDV end-diastolic volume, ESV end-systolic volume, EF ejection fraction, LVM left ventricular mass, max. IVS maximal thickness of the interventricular septum, BSA body surface area.

[a] 9–18 h sports activity/week.

[b] 18 h sports activity/week.

[c] Calculated as mean ± 2*SD.

Table 2
Right ventricular parameters, adapted from *"Reference ranges ("normal values") for cardiovascular magnetic resonance in adults and children: 2020 update.*

Parameter	Non-athletes [mean ± SD (LL–UL)[c]]		Regular athletes[a] [mean ± SD (LL–UL)[c]]		Elite athletes[b] [mean ± SD (LL–UL)[c]]	
	Men	Women	Men	Women	Men	Women
RVEDV (ml)	223 ± 40 (143–303)	166 ± 23 (120–212)	277 ± 36 (205–349)	209 ± 29 (151–267)	291 ± 48 (195–387)	219 ± 35 (149–289)
RVEDV/BSA (ml/m^2)	111 ± 18 (75–147)	96 ± 12 (72–120)	136 ± 16 (104–168)	115 ± 15 (85–145)	144 ± 20 (104–184)	118 ± 17 (84–152)
RVEDV (ml)	108 ± 24 (60–156)	75 ± 13 (49–101)	135 ± 25 (85–185)	102 ± 17 (68–136)	148 ± 30 (88–208)	103 ± 24 (55–151)
RVEDV/BSA (ml/m^2)	54 ± 12 (30–78)	43 ± 7 (29–57)	66 ± 12 (42–90)	57 ± 9 (39–75)	73 ± 13 (47–99)	56 ± 13 (30–82)
RVM (g)	23 ± 5 (13–33)	18 ± 4 (10–26)	29 ± 6 (17–41)	23 ± 4 (15–31)	30 ± 6 (18–42)	25 ± 5 (15–35)
RVM/BSA (g/m^2)	12 ± 2 (8–16)	10 ± 2 (6–14)	14 ± 3 (8–20)	13 ± 2 (9–17)	15 ± 2 (11–19)	14 ± 3 (8–20)
RVEF (%)	52 ± 5 (42–62)	55 ± 5 (45–65)	51 ± 4 (43–59)	51 ± 4 (43–59)	50 ± 4 (42–58)	53 ± 7 (39–67)

SD standard deviation, LL lower limit, UL upper limit, n number of study subjects, RV left ventricular, EDV end-diastolic volume, ESV end-systolic volume, EF ejection fraction, RVM right ventricular mass, max. BSA body surface area.
[a] 9–18 h sports activity/week.
[b] 18 h sports activity/week.
[c] Calculated as mean ± 2*SD.

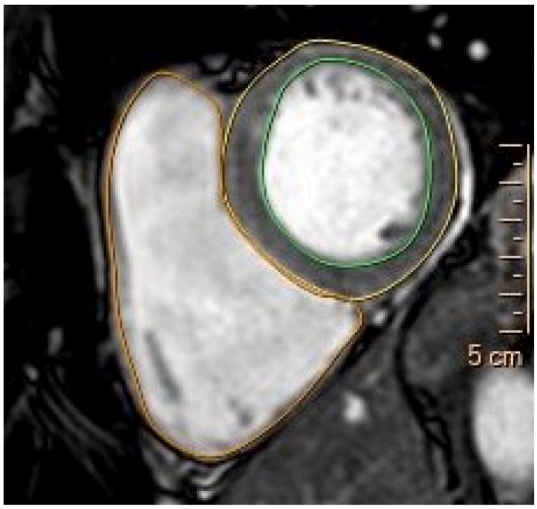

Fig. 1. SSFP, short axis view: example of LV and RV contouring process in the diastolic phase.

and inferior wall at mid-ventricular level >1.3, with any other possible cause of LV hypertrophy excluded (e.g., systemic hypertension, aortic valve stenosis or infiltrative cardiomyopathies) [3,6,26–28]. Few differences in left ventricle myocardial thickness are reported in relationship to ethnicity [21]. In first-degrees relatives of people with diagnosed HCM, LV wall thickness ≥13 mm is considered diagnostic [29].

CMR represents an important diagnostic tool and has a complementary role to echocardiography in the diagnosis and risk stratification of HCM, since the possibility to characterize the precise location, extension, and grade of left ventricular hypertrophy, but also to identify hypertrophic segments not visible by echocardiography (e.g., apex and inferior septum) and to give a tissue characterization [6,26]. For these reasons, at least one CMR is usually performed in every patient with suspected or known HCM [26].

The most typical hypertrophic pattern in HCM is the septal asymmetric form, even if less other common patterns of hypertrophy are possible (apical, concentric, mid ventricular, mass like, lateral wall and RV forms) [6,27] (Fig. 2).

The presence of septal hypertrophy promotes the development of high left ventricular outflow tract (LVOT). This leads to a "suction" effect (Venturi effect) and to the traction of the anterior leaflet of mitral valve (SAM, systolic anterior motion) towards the interventricular septum, with resultant arise of subaortic systolic gradient and LVOT obstruction [27] (Fig. 3). SAM of the mitral valve leaflets with resulting obstruction of LVOT is present at rest in almost 1/3 of patients with HCM [6]; the other 2/3 may experience LVOT during maneuvers that modify loading conditions and left ventricular contractility or are included in the non-obstructive form of HCM [6,30]. SAM can be combined with abnormal structure of the valve itself, like displacement or papillary muscle hypertrophy and elongated mitral leaflet [3]. Using phase contrast imaging it is possible to measure the peak LVOT flow velocity and thus to derive the pressure gradient arising from the LVOT [3]. A gradient value ≥ 30 mmHg is considered diagnostic for the obstructive form of HCM, which is accepted to be a prognostic value: particularly, non-obstructive HCM has usually better prognosis [3,27]. Since the correct

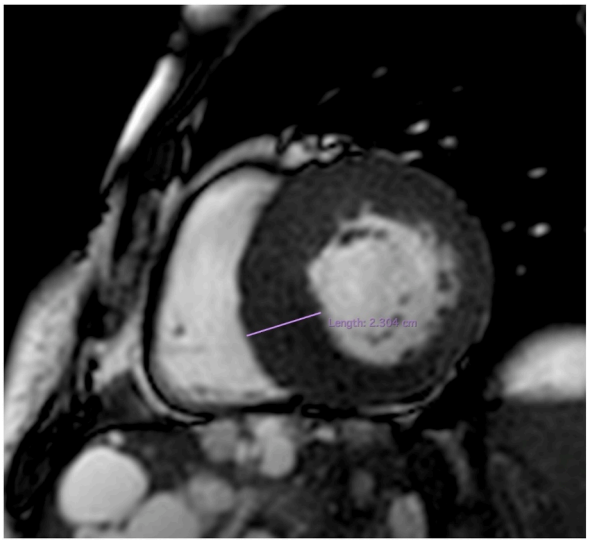

Fig. 2. SSFP, short axis view: interventricular septum hypertrophy (23 mm) in patient with HCM.

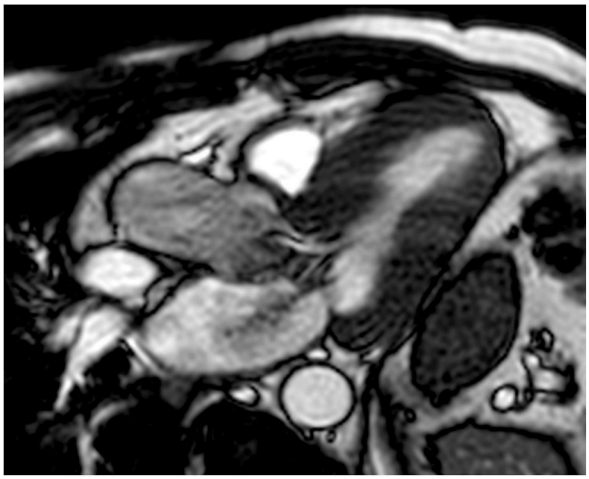

Fig. 3. SSFP long-axis, 3-chamber view: SAM at the level of LVOT in a patient with HCM.

procedure to align the imaging plane to determine the highest flow velocities requires time and has significant risk for errors and giving the fact that is difficult to quantify the turbulent flow and the possibility to measure LV outflow only at rest, Doppler echocardiography remains the first choice in the evaluation of LVOTO [6]. Even if echocardiography has an important role in determining these factors, kinetic alterations are still detectable by MRI imaging, showing regional hypo-contractility before hypertrophy becomes visible [3].

Possible ancillary CMR findings of HCM include alterations of RV wall, in mitral valve, papillary muscles and in myocardial architecture. RV thickening (8 mm or more) is present in more than a third of the cases, mostly at the junction point of RV wall and the anterior or inferior septum. It is possible to detect also prominent RV structures such as crista supraventricularis [6]. In almost one third of HCM cases mitral valve presents increase length of the anterior leaflet ($\geq$30 mm) or of the posterior one ($\geq$17 mm): this alteration contributes to the genesis of sub-aortic gradients. Papillary muscles present alterations in a great subset of patients, particularly regarding number, apical displacement, or anomalous insertion on the anterior mitral valve leaflet [6]. Myocardial crypts (defined as clefts in the LV wall of myocardium), located mostly to the basal inferior septum and LV free wall, show higher prevalence in patients with HCM, but also in patients with genetic alterations of HCM but without alterations typical for the disease [6].

HCM is characterized by structural micro-alterations, such as disarray of myocardial cells or alterations of coronary vascularization with consequent silent microvascular ischemia and increased myocardial fibrosis [31,32], which can lead to higher risk of arrythmias, particularly ventricular tachyarrhythmias/fibrillation, which are the leading cause of SDC in patients with HCM [6]. The microvascular disfunction in HCM patients is responsible for approximately 3% of myocardial infarction with non-obstructive coronary arteries (MINOCA) [33]. Fibrosis is supposed to be represented by LGE on MRI imaging: it is present in almost 50% of patients with HCM, involving about 10% of myocardial volume. Typically, LGE has a mid-wall distribution, mostly located on the anterior free wall and on

the insertion of RV on interventricular sept, known as hinge point [3,6,34]. More recently LGE has been considered a risk factor to identify higher-risk patients, in addition to the traditional risk factors (massive LV hypertropia, familiarity for SDC and syncope). Particularly, extensive LGE (involving >15% of the LV total mass) seems to be linked to higher risk of cardiac adverse events and can help in identifying high-risk patients in absence of the other traditional risk factors [6]. LGE can be useful in the early identification of the small subset of patients that will likely develop an end-stage HCM, with an increased myocardial fibrosis that leads to LV remodeling and systolic disfunction [35]. The presence of fibrosis may be used to distinguish between HCM and physiological adaptations in athletes, even if LGE could be absent in HCM, especially in young patients and in those with moderate disease [29]. The evaluation of native T1 mapping can be used to assess and quantify the myocardial fibrosis, helping to discriminate between these diseases [26].

Cardiac MRI can be also crucial in detecting less typical form of HCM, such as the apical one, hardly discovered by echocardiography and potentially associated with the development of wall thinning and apical aneurysm, also included in the high-risk group of SCD [3,36]. Other less frequent forms of HCM are the focal ones; it is important to distinguish these forms of cardiac hypertrophy from cardiac masses or pseudo masses. The correct CMR protocol provides not only the characterisation of the tissue, but also information about its vascularization, its relations with the surrounding structures, and identifies myocardial contractility in case of focal hypertrophy [8,37].

The use of more recent mapping techniques is useful in the characterization of HCM. It is well known that native T1 mapping (nT1) is mildly and diffusely increased in patients with HCM (involving also segments with no signs of fibrosis), with the highest values in hypertrophic segments of LV and in those with LGE [4]. It has also been shown that elevation of nT1 and T2 mapping values manifests early in HCM pathogenesis, even before the appearance of wall thickness and LV disfunction, thus highlighting that mapping techniques can have an important role in the diagnosis of HCM at early stages [4]. Elevation of T2 mapping values is reported by Amano et al. to be able in distinguish the more aggressive forms of HCM, characterized by major myocardial injury [4]. In HCM patients also ECV (extracellular volume) values are elevated, correlating with LGE percentage. For these reasons it is recommended that CMR protocol in patients with HCM comprises a complete mapping evaluation [4].

5. Athlete's heart

Persistent training in athletes causes a series of adaptive alterations in the heart as response to sustained high workload conditions [38]. Athlete's heart (AH) refers to a clinical condition characterized by specific cardiac modifications driven by a regular physical training, as consequence of hemodynamic changes related to heart rate (HR) reduction, stroke volume (SV) increase with a usually normal or slightly reduced ejection fraction at rest and good contractile reserve, as well as reduction in the systemic vascular resistance [28,39]. This condition is dominated by LV dilatation and athlete's hypertrophy of the left ventricle [39]. The range of remodeling relies on period of training and intensity, but also on athlete's blood pressure during training [38].

It is well established that regular training conveys cardiovascular benefits; AH has not been associated with significant risks for the athlete, but it has overlapping morphological features with other high risk and life-threatening conditions including HCM, hence the importance of differential diagnosis of the cause of LVH [38,39].

It is possible to distinguish between physiological changes occurring in athlete's heart and other cardiac disorders using a multimodality imaging approach [39]. CMR can evaluate cardiac function and morphology, quantify volumes, and flow and operate tissue characterization, hence it represents a powerful diagnostic tool to identify AH [40].

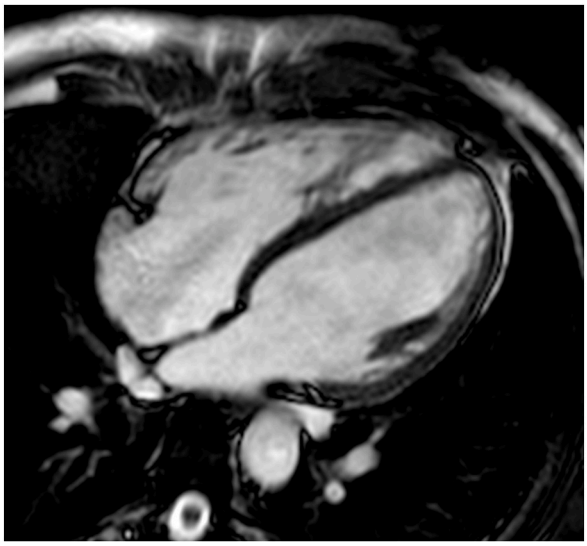

Fig. 4. SSFP long-axis, 4-chamber view: bi-atrial and bi-ventricular dilatation in a patient with athlete's heart.

In AH the hypertrophic pattern depends on the type of training: an eccentric hypertrophy with increased ventricle mass and size is more often present in endurance sports, due to volume overload, while a concentric hypertrophy with increase in ventricle mass without chamber dilation is mainly found in strength sports, caused by pressure overload. It is also possible to find mixed patterns of hypertrophy in athletes who practice mixed type of training [28,38]. AH usually presents with LV symmetrical hypertrophy, while HCM is characterized by asymmetric apical or septal hypertrophy [28] (Fig. 4). In contrast to HCM, AH shows typically LVH regression after a detraining period: diagnosis of AH is supported by the decrease >2 mm of LVH after a three-months period without exercise [28]. Moreover, global and regional systolic and diastolic function is preserved in AH, such as strains and strain rate (which can be mildly reduced in HCM) [28].

Regarding the T1 mapping and ECV values, they are reduced in AH, since in AH hypertrophy is characterized by elevated cellular component and relative reduced extracellular space [28]. Hence, T1 mapping and ECV can be used to improve the diagnosis of AH, especially if LVH has 12–15 mm values [28]. Usually there is no evidence of LGE in AH; rarely it appears as a mesocardiac stria at the anterior or posterior interventricular junctions and at the insertion point of the trabeculae on the ventricular wall [28]. LGE in AH is caused by the high systolic pressure correlated to training it has been reported a correlation between LGE presence and the intensity of exercise [28].

AH shows also, some features overlapping with many other cardiac conditions, such as dilated cardiomyopathy, arrhythmogenic right ventricular cardiomyopathy (ARVC), left ventricular non-compaction and infiltrative cardiomyopathy, so that a correct differential diagnosis can be challenging. In this setting, it is important to know the main radiological features of AH and how it develops [28].

6. Infiltrative heart diseases

6.1. Amyloidosis

Amyloidosis is a multi-systemic disorder caused by the accumulation of insoluble amyloid fibrils in the extracellular space of various tissues and organs, progressively leading to gradual organ failure. Amyloid fibrils originate from more than 30 different precursor proteins [41]. Cardiac involvement is frequently present in systemic amyloidosis, mainly caused by accumulation of two types of protein: immunoglobulin light-chain (AL) and transthyretin (TTR) [41,42]. AL amyloidosis is caused by production of monoclonal light chains by a small B-cell clone, usually a plasma cell clone [43]. In AL amyloidosis heart involvement represents the main cause of death, occurring within a few months if diagnosed at advanced stages [42,43]. Transthyretin amyloidosis (ATTR) is classified in a hereditary form (ATTRm), caused by different mutations in TTR and a non-hereditary form, caused by misfolding of wild-type transthyretin (ATTRwt) also known as "senile systemic amyloidosis", which has late onset and affects more often men [20,41]. In ATTRwt cardiac involvement is usually the only manifestation [42], while ATTRm presentation is variable, depending on the specific mutation (namely, Thr60Ala mutation is often accompanied by cardiomyopathy) as well as patients' age, sex, and ethnicity [42]. ATTR cardiomyopathy (ATTR-CM) shows a better prognosis (overall survival 4–5 years from diagnosis) than the AL-CM (<6 months), thanks to the recent development of effective therapies [42].

In cardiac amyloidosis insoluble amyloid fibrils accumulation leads to diastolic disfunction and restrictive cardiomyopathy [42]. CMR has an important role in the diagnosis of cardiac involvement in systemic amyloidosis [20,41]. ATTR-CM and AL-CM show different morphological phenotypes: the main hypertrophic pattern in ATTR-CM is the asymmetrical LV hypertrophy (present in 79%

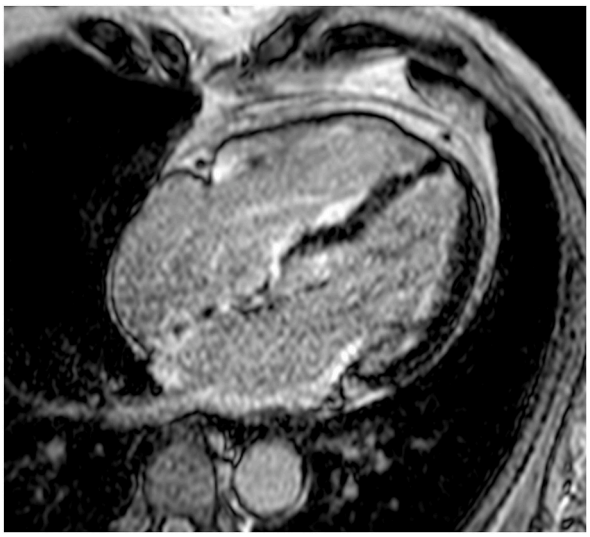

Fig. 5. Inversion recovery sequence to evaluate LGE, 4-chamber view: the image shows diffuse subendocardial LV LGE in a Patient with aTTR amyloidosis with cardiac involvement. LGE is also visible both in left and right atrium.

of patients). Asymmetrical septal hypertrophy can be distinguished into two further morphological variants: sigmoid septum and reverse septal contour, respectively present in 55% and 24% of patients with ATTR-CM, with no significant differences between the two forms of ATTR-CM [20]. The most prevalent form of cardiac remodeling in AL-CM is the symmetrical and concentric LV hypertrophy (present in 68% of patients) [20].

CMR provides structural and functional information about heart involvement in systemic amyloidosis, especially if LGE and mapping techniques are used [20]. LGE in amyloid cardiomyopathy is typically diffuse and subendocardial in early stages and becomes transmural in advanced stages of the disease [20] (Fig. 5). Traditional LGE imaging is a comparison technique that requires the selection of null inversion time by the operator, depending on what is considered normal myocardium; in CA this process can be difficult since the presence of diffuse infiltration of the myocardium and frequent absence of normal areas, possibly leading to null the abnormal myocardium [20]. PSIR (phase-sensitive inversion recovery) is a novel reconstruction technique of LGE images that enables a better determination of cardiac involvement and extension, since it is less sensitive to operator choice of null point and can render truly T1-weighted signal intensity [20]. There are three possible patterns of LGE in CA, which have direct correlation with the degree of cardiac infiltration: LGE can be absent or present with a subendocardial or transmural distribution.

Mapping techniques, particularly native T1 mapping (nT1) and ECV, have been demonstrated to be a surrogate marker of infiltration in CA [41]. ECV and nT1 are typically increased in patients with CA; more recent studies reported that nT1 is higher in AL-CM patients [41]; Fontana et al. founded higher ECV values in patients with ATTR-CM than in those with AL-CM [20,44]. NT1 and ECV correlate with prognosis in patients with amyloid cardiomyopathy, and ECV is and independent factor of prognosis in ATTR-CM and early marker of amyloid regression in patients undergoing therapies in AL amyloidosis [20]. Finally, T2 mapping values are usually increased in patients with both forms of cardiac amyloidosis, identifying myocardial oedema [20] (Fig. 6, panel A and B example of nT1 mapping, Fig. 7, panel A and B example of T2 mapping).

Different studies reported a significative prevalence of ATTR-CA in patients with aortic stenosis (AS) who undergo transcatheter aortic valve replacement (TAVR), approximately 6% for patients >65 years, with higher percentages in older people [45–47]. Patients with bot CA and AS reported a worse prognosis after TAVR than those without CA [46,47]. Since patients with AS undergo a CCT as part of routine TAVR evaluation to define annulus dimension, vascular access, and coronary artery height, cardiac CT can be used also to identify myocardial ECV to help clinicians to diagnose occult cardiac amyloid deposition (ECV values are massively increased in CA), with important implications in the management of those patients [48].

6.2. Sarcoidosis

Sarcoidosis is a non-caseating granulomatous multisystemic disease that affects multiple organs, particularly the lymphatic system, lungs, skin, eyes, and nervous system. Cardiac symptomatic involvement has been reported in approximately 5% of patients, even if in few autoptic studies cardiac involvement have been reported in 25% of cases. Cardiac involvement is clinically silent in most patients, but some ECG signs may guide the diagnosis, such as complete heart block and ventricular arrhythmias, right bundle branch block, and SDC [49]. Since cardiac sarcoidosis (CS) is responsible for morbidity and mortality, early diagnosis is important to prevent severe consequences; it also guides corticosteroid therapy to prevent cardiac arrhythmias and to improve LV function [49,50].

Cardiac involvement occurs in the typical three stages of the disease: acute myocardial inflammation, post-inflammatory pattern, and replacement scarring [50]. CMR represents a crucial non-invasive and advanced imaging test with a diagnostic and prognostic

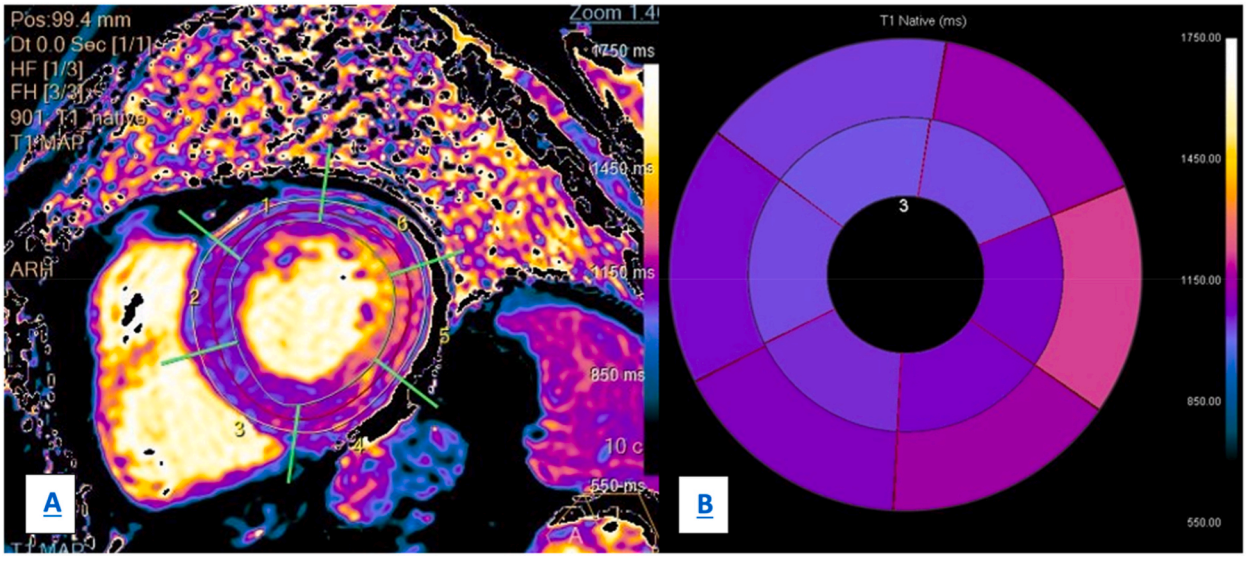

Fig. 6. Native T1 mapping, panel A shows the segmentation process to calculate nT1 values in the same patient in Fig. 5. Panel B (bull's eye) shows the results: nT1 values are elevated (within 1213 ms).

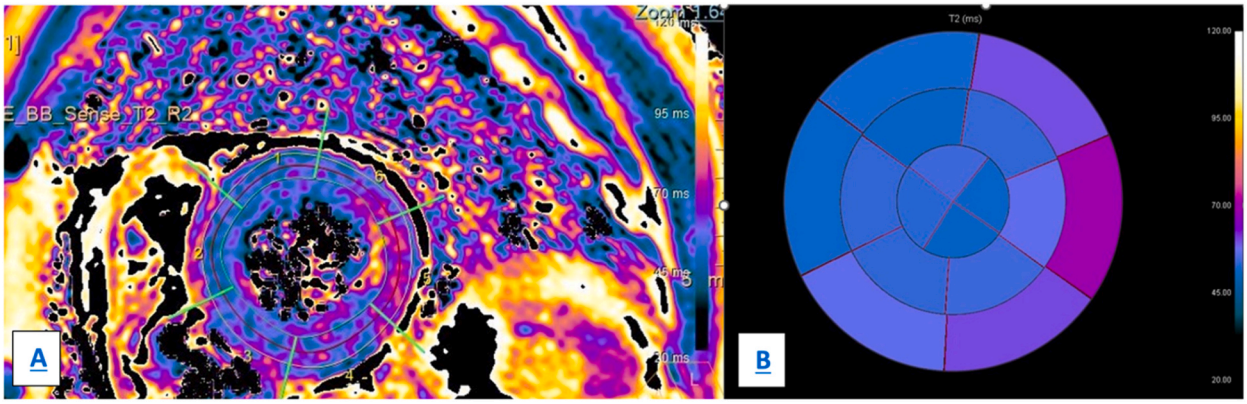

Fig. 7. T2 mapping. Panel A shows the segmentation process, panel B (bull's eye) shows the resulting values of T2 mapping, increased.

value, able to reach an early diagnosis of CS [49,51], because of the high spatial resolution and the ability of evaluating left and right ventricular function, combined with tissue characterization [51]. Typical findings in patients with ongoing acute phase are wall motion anomalies non corresponding to coronary distribution, LV wall thickness accompanied by signal hyperintensity on T2-weighted imaging, correlated to inflammation [49]. In the chronic phase of CS and in inactive disease, wall thinning, or aneurysm can be detected, with hypointense signal in T2-weighted imaging and presence of LGE as a sign of fibrosis [49,51]. The typical LGE in CS is at the level of septal and lateral wall of basal segments [51], with a mid-myocardial or subepicardial patchy pattern (non-ischemic distribution), but it is possible to find in few cases a subendocardial pattern, mimicking a prior myocardial ischemia [52]. LGE in patients with suspected or confirmed CS is correlated with adverse prognosis, since it is related to cardiovascular events such as ventricular arrythmias and SDC [52] (Fig. 8).

The LGE evaluation has some limitations, particularly it is less sensitive in detecting active myocardial inflammation, so at present time it is not properly used to guide the therapy [51,53]. Novel CMR techniques of myocardial mapping have been shown to allow the detection of myocardial inflammation and to improve the diagnosis of silent CS [49,51]. Some studies showed that patients with CS had significantly higher values of T1, T2 and extracellular volume compared to heathy people [49,54,55].

The final diagnosis of sarcoidosis is made up with anatomopathological criteria and diagnostic imaging modalities; CMR and mapping techniques are helpful to improve the accuracy [56]. Nowadays several hybrid techniques such as PET-CMR seem to be able to identify new granulomatous lesions and patients at high risk of adverse events, therefore it should be considered when assessing disease presence, stage, and prognosis in CS [52]. Moreover, in patients with sarcoidosis it is possible to detect cardiac involvement performing cardiac CT: the iodine-based CT contrast accumulates in myocardial scars in a similar manner as gadolinium-based MRI

Fig. 8. Inversion recovery sequence to evaluate LGE, short axis view: patient with history of isolated cardiac sarcoidosis. Short axis view shows LGE at the inferior hinge point at medium level on the infero-septal wall of LV.

contrast agents, thus providing myocardial fibrosis assessment in those patients who are ineligible for CMR [57].

6.3. Fabry-Anderson disease

Fabry-Anderson disease (AFD) is a rare X-linked autosomal recessive multisystemic lysosomal storage disease, with incidence of approximately 1/50.000 individuals [58], related to a mutation in the α-galactosidase gene, which leads to the lysosomal accumulation of glycosphingolipids in several tissues and organs, potentially resulting in cardiac, cerebral, and renal impairment [59]. Although AFD is an X-linked transmitted disease, it has been demonstrated that even heterozygous females can be affected [60]. Different types of AFD have been distinguished: the classical phenotype (characterized by the complete absence of the enzyme) and some with only reduction in α-galactosidase activity. In the latter group is included a cardiac variant similar to hypertrophic cardiomyopathy, that may express only with LVH in the absence of other signs of the disease. Usually, AFD manifests itself in the third decade of life in men and may persist asymptomatic until much later in women [61]. Men with the classical form of Fabry disease are diagnosed early and show a variety of clinical manifestations, including peripheral neuropathy, skin lesions, and nephropathy with early proteinuria and progression to renal dysfunction [62]. Although the diagnosis of AFD is often delayed, a prompt start of enzyme replacement therapy (ERT) has a significant impact on the prognosis, since ERT inhibits the initiation and progression of myocardial damage, which represents the main cause of death in these patients [61,63]. Regarding cardiac involvement, it starts early and progresses not accompanied by significant symptoms, usually with LVH that mimics HCM, with different degrees in wall thickening. Myocardial storage leads to progressive diastolic dysfunction. Moreover, the involvement of intramural vessels causes functional and structural alterations which lead to myocardial ischemia [63]. The development of replacement fibrosis, commonly identified on the posterior-lateral wall at basal level, and afterload alterations (associated with FD vasculopathy) cause an increase in LV volume, making it more spherical. These alterations may lately lead to arrhythmias or heart failure [58]. At echocardiography evaluation AFD disease alterations are similar to many other HCM diseases, and the differential diagnosis may be difficult in most cases if not supported by specific ECG signs, positive family history, or other signs of AFD [64]. CMR has rapidly become a crucial tool in the early diagnosis and staging of FD [63]. Particularly, LGE has been found in up to 50% of AFD patients and, along with maximum wall thickness and cardiac mass, it has been recognized as the best predictor of cardiac events, since it often precedes the development of LVH [65]. LGE has been described as myocardial fibrosis due to local imbalance between increased collagen synthesis and decreased metalloproteinases caused by glycosphingolipids [65]. The typical LGE in AFD is located at the basal-inferolateral mid-wall with subendocardial sparing, but it is possible to find more diffuse LGE in case of severe LVH [58,66]. The typical LGE distribution helps in the differential diagnosis of LVH [66].

T1 mapping provides tissue characterization to differentiate LVH causes. Particularly, myocardial nT1 values show a global shortening in AFD because of myocardial storage of glycosphingolipids, as the T1 of fat tissue is very low [66,67], differing from other infiltrative cardiomyopathies with normal or elongated nT1 values [1,68] (Fig. 9, panel A and B example of nT1 mapping). Some studies reported that in AFD without LVH, nT1 values were significantly lower than in other caused of LVH and other studies found T1 mapping anomalies in AFD patients with no LVH [61,67,68]. This supports the role of nT1 values in providing an independent incremental diagnostic tool beyond age, gender, and traditional imaging features [1,68]. It is important that myocardial T1 map is interpreted with attention since the pathology of cardiac involvement in AFD is progressive: inflammation, hypertrophic changes and fibrosis follow the starting sphingolipid deposition, so that T1 relaxation times may be normal (the so called "pseudo normalization of T1 times") in areas with both sphingolipid storage and fibrosis [61]. T2 mapping values are usually increased in cardiac AFD, correlating with chronic inflammatory cardiomyopathy [61,69]. For these reasons both T1 and T2 mapping should be always performed in case of AFD (both suspected and confirmed) and in the monitoring of the disease progression [61].

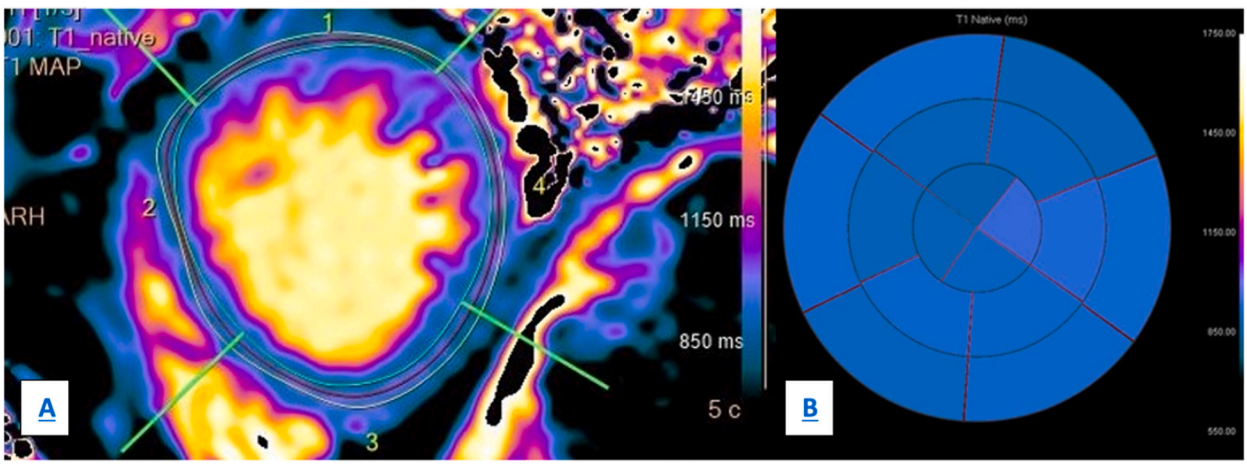

Fig. 9. Native T1 mapping, panel A shows the segmentation process to calculate nT1 values in a patient with Fabry disease; panel B (bull's eye) shows the results: the mean values are mildly reduced.

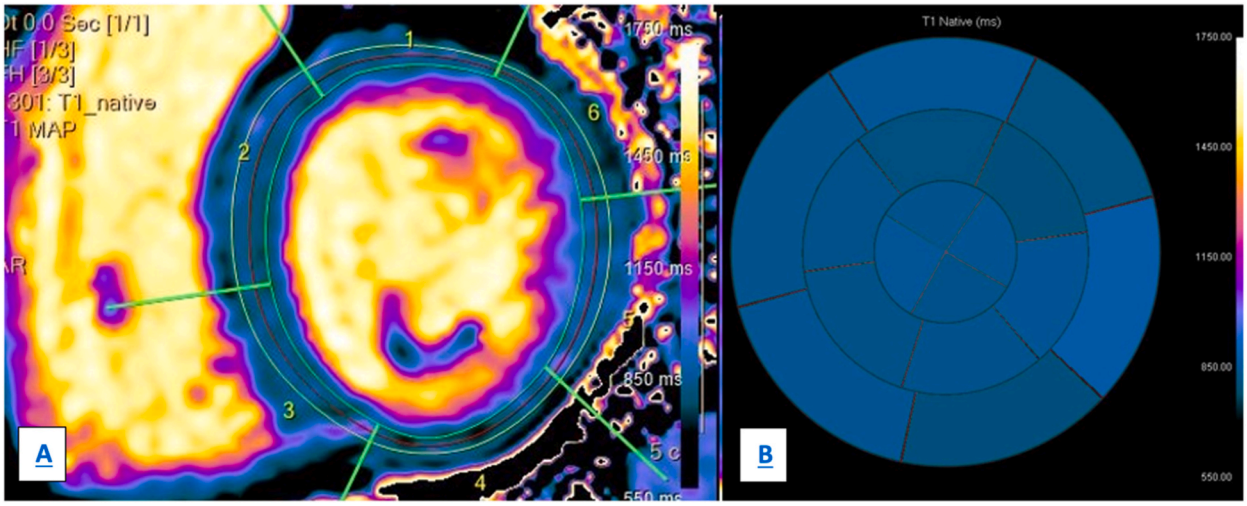

Fig. 10. Native T1 mapping, panel A shows the segmentation process to evaluate nT1 values in a patient affected by cardiac iron overload. Panel B (bull's eye) shows the results: nT1 values are reduced (819–842 ms).

The possible role of CMR in evaluating the response to ERT therapy is still under investigation but some studies showed that it is superior to echocardiography in the assessment of LVH [70] and that ERT induces reductions in myocardial T2 values and left ventricular mass and wall thickness in patients with only little or no LGE at all at baseline [61,71,72]. It has also been reported that in patients with FD associated with LVH there is a small but detectable decrease in LV mass and partial normalization of T1 mapping values after one year from ERT start, thus highlighting the role of T1 mapping in the evaluation of post-treatment changes in myocardial glycosphingolipid storage [73].

6.4. Lysosomal storage disorders

Lysosomal storage disorders (LSDs) are a heterogeneous group of more than 50 genetic disorders caused by lacking proteins involved in lysosomal metabolism, such as lysosome enzymes or membrane transporters [74], due to mutations in genes that encode for lysosomal glycosidases, integral membrane proteins, enzyme modifiers or activators, transporters, or proteases. Most of the forms are transmitted as autosomal recessive trait [74], but three (Anderson Fabry disease, Danon disease, and mucopolysaccharidosis (MPS) type II, also known as Hunter disease) are X-linked. Mutated proteins are dysfunctional and cause lysosomal malfunction and progressive storage of proteins inside the lysosome, leading consequently to cell death [75]. The classification of LSDs is based on the type of material stored, e.g., lipid storage disorders, MPS, and glycoproteinoses [74]. Although they are uncommon one by one, LSDs have an incidence from 1/5000 to 1/5500, the highest for Fabry disease (2.5/100000 males), Gaucher disease (2/100000 males) and Pompe disease (2.5/100000) [75]. LSDs are usually multi-organ disorders and can be symptomatic from the prenatal period to adulthood [75]. Cardiac involvement is present mostly in Pompe disease and Danon Disease (glycogen storage disease type IIa and IIb, respectively), MPS and Anderson-Fabry disease, with different possible manifestations (from coronary artery disease to valvular disease or dilated or hypertrophic cardiomyopathy) [74]. Most LSDs are diagnosed by detecting a specific enzyme absence; genetic exams can help confirming the diagnosis [74].

Glycogen storage disease type IIa, also known as Pompe disease, is caused by α-1,4-glucosidase (GAA) deficiency, leading to lysosomal storage of glycogen in the tissues, particularly in skeletal muscle, respiratory muscle, and the heart [74,76]. The severity of disease depends on age of onset, rate of progression and burden of organ involvement [76]. The early infantile-onset form, caused by complete or almost-complete absence of GAA, has estimated incidence of 1/138,000 [74] and shows severe cardiomyopathy, respiratory and cardiac failure, associated with quadriplegia; this form has a very bad prognosis beyond one year in absence of prompt enzyme replacement therapy [76]. The other two forms of Pompe disease (juvenile and adult forms) are caused by reduction but somehow residual GAA activity, have later onset (first decade of life for the juvenile form, third to sixth decade for the adult form), slower progression of skeletal weakness and absence or only moderate presence of cardiac involvement [74].

Cardiac involvement in Pompe disease causes heart enlargement, thickening of all chambers, particularly the LV free wall and the papillary muscles. In advanced diseases, there may be also small cardiac cavities and obstruction to left or right ventricular outflow. Some patients show dilatation of cardiac chambers [74]. The use of CMR in young patients with Pompe disease is rarely performed, due to the elevated risk associated to sedation in these patients. However, it has been shown that CMR can be an appropriate tool in the follow-up of patients undergoing ERT, especially regarding the myocardial response to therapy, even without sedation [77]. In the late-onset form of Pompe disease only few studies have reported mild or nonspecific cardiac alteration on CMR imaging (particularly, LGE with non-ischemic pattern in the basal LV inferolateral wall, increased ECV values suggesting interstitial fibrosis, left atrial dilatation in only few patients). These alterations were mostly associated to the overlap between the storage disease and other comorbidities [76].

Danon disease (DD) represents a rare vacuolar myopathy caused by the LAMP2 (Lysosomal Associated Membrane Protein-2) deficiency. DD is transmitted as X-linked trait and shows high penetrance. The main clinical manifestations of DD are the early LAMP2 cardiomyopathy, which usually emerges as SDC, early onset heart failure or arrhythmias, Wolff Parkinson-White syndrome, skeletal myopathy, retinopathy, and cognitive impairment [78,79]. Patients with DD may be eligible for heart transplant, implantable cardioverter-defibrillator (ICD) and some targeted therapies trials [79]. Usually, male patients have earlier onset and more aggressive cardiac involvement than female, but a severe arrhythmogenic phenotype has been described also in women [80].

Since DD is a rare condition, it is not uncommon that DD cardiomyopathy is confused with HCM or other causes of left ventricular hypertrophy [79,80]. Some case reports described cardiac findings in patients with DD [78–80]: few patients showed HCM phenotype and LGE with pattern not typical for other causes of left ventricular hypertrophy, suggesting that genetic testing for LAMP2 mutations should be performed in these cases, especially if other clinical features typical for DD are present (e.g., Wolff-Parkinson-White syndrome or cognitive disorder) [80]. It is also reported that male patients present more frequently LV concentric hypertrophy [79], while female patients may present with asymmetric LVH, associated with RV hypertrophy, less severe forms of HCM or also with a DCM phenotype [78,79]. Other prevalent findings in females were LGE at the insertion sites at the LV-RV and right ventricular. Even if the LGE patterns and cardiac alterations are variable, it is reported that the mid-interventricular septum is always spared. CMR findings may contribute to raise DD imaging suspicion in HCM and DCM phenotypes [79].

Mucopolysaccharidosis (MPSs) are caused by lack of enzymes that degrade glycosaminoglycans (GAGs), leading to gradual deposition of GAGs in tissue and organs and in the end to multi-systemic failure. Cardiac involvement is reported in all MPSs; it is particularly common and early-onset in MPS I, II and VI. In MPS cardiac involvement is characterized by cardiac valve thickening, valve dysfunction (especially left-sided) and hypertrophy. There may be also alterations in the conduction system, as well as coronary artery and vascular involvement. Cardiac disorder causes early mortality [81]. There are only few reports of CMR findings in patients with MPS, showing thickness and stiffness of the posterior mitral leaflet and of the anterior tricuspid leaflet, dilatation and hypokinesis of RV and paradox motion of the septum, without signs of LGE and fibrosis [82].

6.5. Iron overload

Iron overload counts a group of disorders characterized by systemic iron overload (IO) [83].

Primary IO is caused by mutations in genes that regulate iron absorption (hereditary hemochromatosis), while the secondary form is caused by iron iatrogenic overload (iron administration or repeated red blood cell transfusions), haematological disorders that lead to non-effective erythropoiesis or liver diseases [84]. Excess body iron may accumulate in different organs and lead to complications such as heart failure, cardiac arrhythmia, liver fibrosis and endocrine diseases [85,86].

In cardiac involvement iron overload can lead to iron overload cardiomyopathy (IOC), which is the leading cause of death in iron overloaded patients, resulting in cardiac dysfunction, originally diastolic and then systolic, due to iron deposition in the myocardium [86]. Iron overload in the myocytes is a progressive process which begins in the perinuclear lysosomes and proceeds in the sarcoplasm as serum iron levels increase. Myocardial iron deposition starts from epicardium and extends toward endocardium, explaining the systolic function maintenance until late phases of the disease [59]. Clinical manifestations of IOC vary from asymptomatic patients to irreversible heart failure symptoms in severely overloaded patients with dilated cardiomyopathy [86]. Iron deposition can also arise in the pericardium and in the conduction system with possible signs and symptoms and arrythmias [59,86].

Iron overload diagnosis is challenging and accurate IO evaluation in specific organs is helpful in planning treatment [86]. Different examinations have been proposed to identify cardiac iron overload: there is evidence that although serum iron studies are useful to screen total-body iron overload, they are not a diagnostic tool to find organ specific overload. Invasive procedures such as cardiac biopsy are not useful in screening asymptomatic patients. Moreover, cardiac iron deposition is not homogeneous so that biopsies could miss the areas of deposition. Echocardiography can detect some early alterations due to iron overload but is not sensitive to detect definite iron deposition.

At present time, CMR represents the most powerful tool to detect and quantify cardiac iron overload by myocardial T2* MR quantification [86,87]. In iron overloaded hearts the paramagnetic effect of iron is responsible for changes in MR signal intensity, shortening T1 and T2 relaxation times [59]. Using gradient echo sequences (which are more susceptible to magnetic field inhomogeneity and particularly affected by aggregated particles of hemosiderin iron) T2* value can be measured and derived by fitting signal intensities of left ventricular myocardium regions of interests (ROI) in the interventricular septum at different echo times to a mono-exponential equation [87,88]. Using the T2* value people with IOC are divided into three groups, each of which correlates with the severity of IOC itself. T2*>20 ms values (green zone) reflect no iron overload, with low risk for the imminent evolution to congestive heart failure. T2* values from 10 to 20 ms (yellow zone) are associated with mild to moderate iron load and patients are at intermediate risk of cardiac failure. T2*<10 ms (red zone) reflects severe iron load and patients are at high risk of cardiac decompensation, needing prompt intensification of the therapy [86,87]. T2* monitoring has also a crucial role in monitoring the iron overload status during the chelation therapy [86] (Fig. 10, panel A and B example of nT1 mapping; Fig. 11, panel A and B, example of T2* analisys).

Even if iron overload is detected with T2* technique, T1 mapping and ECV measurement may give some additional information to better identify left ventricular impairment and cardiac iron overload. T1 mapping has been associated with a better reproducibility than T2* measurements in patients with only mild iron cardiac load [87,88].

Cardiac magnetic resonance has also a crucial role in the measurement of left and right ventricular indices [89]. LVEF (left ventricular ejection fraction) is the reference standard of the systolic function, but its sensitivity to detect cardiomyopathy in IO is limited to later phases of the disease. On the contrary, strain analysis can assess the contractile cardiac function even at the earliest subclinical

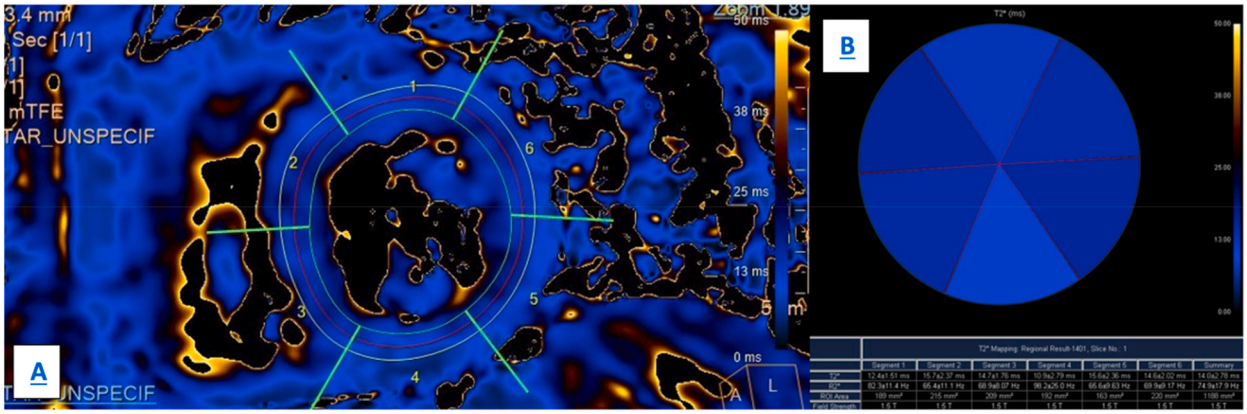

Fig. 11. T2* mapping, panel A shows the segmentation process to calculate the T2* values in the same patient of Fig. 10. Resulting values are shown in panel B: mean T2* values are low (15 ms, normal range >20 ms).

stages [90]. It has been shown that myocardial strain by feature-tracking (FT) CMR is associated with myocardial T2* and can predict with high sensitivity the systolic disfunction and myocardial fibril deformation by detecting the strain values in patients with cardiac IO with T2* levels >20 ms (in a normal range) [90,91].

7. Conclusions

Hypertrophic heart phenotype is present in different pathological and para-physiological conditions. CMR currently plays different key-roles in the diagnostic and prognostic workflow of cardiac hypertrophy and has become routinely part of cardiac hypertrophic heart evaluation. First, it contributes to the differential diagnosis of LVH. Particularly, it can differentiate between real cardiac hypertrophic heart from cardiac masses or pseudo masses and, in presence of confirmed cardiac hypertrophy, it has the ability both to evaluate the kinetical function of the heart and to characterize tissues (particularly studying LGE patterns and using novel mapping techniques). This provides strong confidence in the diagnosis of the cause of hypertrophy.

Tissue characterization has also an important role as a prognostic factor in case of LVH: it is especially evident for the evaluation of LGE, since LGE presence and extension impact negatively on prognosis of different cardiomyopathies (e.g., HCM), being associated to the presence of fibrosis, and thus to higher risk of cardiac events. Moreover, CMR is routinely used to stratify the gravity of some diseases, thus becoming a powerful diagnostic tool to refer patients to therapy (e.g., cardiac iron overload). In some cardiomyopathies it has also a role in the evaluation of response to treatment (e.g., iron overload, Fabry disease).

Author contribution statement

Conceptualization, writing–review and editing, D.T., R.F., C.G., P.F. and M.G.; Writing–original draft, C.G., E.B., A.B., A.C., F.M., M.M., F.P.P. and M.T.

Funding statement

No funding was received for this work.

Data availability statement

N/A.

Declaration of competing interest

The authors declare the following financial interests/personal relationships which may be considered as potential competing interests:Marco Gatti MD is a Guest editor for Heliyon Clinical Research.

References

[1] S. Pradella, G. Grazzini, C. de Amicis, M. Letteriello, M. Acquafresca, V. Miele, Cardiac magnetic resonance in hypertrophic and dilated cardiomyopathies, Radiologia Medica 125 (2020) 1056–1071, https://doi.org/10.1007/s11547-020-01276-x.

[2] M. Stachera, P. Przybyło, K. Sznajder, M. Gierlotka, Cardiac magnetic resonance in the assessment of hypertrophic cardiomyopathy phenotypes and stages – pictorial review, Pol. J. Radiol. 86 (2021) 672–684, https://doi.org/10.5114/pjr.2021.112310.

[3] R.D. Proctor, J.S. Shambrook, P. McParland, C.R. Peebles, I.W. Brown, S.P. Harden, Imaging hypertrophic heart diseases with cardiovascular MR, Clin. Radiol. 66 (2011) 176–186, https://doi.org/10.1016/j.crad.2010.09.008.

[4] A. Baggiano, A. del Torto, M. Guglielmo, G. Muscogiuri, L. Fusini, M. Babbaro, A. Collevecchio, R. Mollace, S. Scafuri, S. Mushtaq, E. Conte, A.D. Annoni, A. Formenti, M.E. Mancini, G. Mostardini, D. Andreini, A.I. Guaricci, M. Pepi, M. Fontana, G. Pontone, Role of CMR mapping techniques in cardiac hypertrophic phenotype, Diagnostics 10 (2020), https://doi.org/10.3390/diagnostics10100770.

[5] M. Chinali, G.P. Aurigemma, Editorial: refining patterns of left ventricular hypertrophy using cardiac MRI: "Brother, can you spare a paradigm? Circ Cardiovasc Imaging 3 (2010) 129–131, https://doi.org/10.1161/CIRCIMAGING.110.944959.

[6] K.G. Grajewski, J. Stojanovska, E.S.H. Ibrahim, M. Sayyouh, A. Attili, Left ventricular hypertrophy: evaluation with cardiac MRI, Curr. Probl. Diagn. Radiol. 49 (2020) 460–475, https://doi.org/10.1067/j.cpradiol.2019.09.005.

[7] E. Conte, S. Mushtaq, G. Muscogiuri, A. Formenti, A. Annoni, E. Mancini, F. Ricci, E. Melotti, C. Gigante, Z. Lorenza, M. Guglielmo, A. Baggiano, R. Maragna, C. M. Giacari, C. Carbucicchio, V. Catto, M. Pepi, D. Andreini, G. Pontone, The potential role of cardiac CT in the evaluation of patients with known or suspected cardiomyopathy: from traditional indications to novel clinical applications, Front Cardiovasc Med 8 (2021), https://doi.org/10.3389/fcvm.2021.709124.

[8] D.C.L. de Oliveira, F.B. Assunção, A.A.S.M.D. dos Santos, M.S. Nacif, Cardiac magnetic resonance and computed tomography in hypertrophic cardiomyopathy: an update, Arq. Bras. Cardiol. 107 (2016) 163–172, https://doi.org/10.5935/abc.20160081.

[9] E. di Cesare, S. Carerj, A. Palmisano, M.L. Carerj, F. Catapano, D. Vignale, A. di Cesare, G. Milanese, N. Sverzellati, M. Francone, A. Esposito, Multimodality imaging in chronic heart failure, Radiologia Medica 126 (2021) 231–242, https://doi.org/10.1007/s11547-020-01245-4.

[10] C.T. Arendt, R. Czwikla, L. Lenga, J.L. Wichmann, M.H. Albrecht, C. Booz, S.S. Martin, D. Leithner, P. Tischendorf, A. Blandino, T.J. Vogl, T. D'Angelo, Improved coronary artery contrast enhancement using noise-optimised virtual monoenergetic imaging from dual-source dual-energy computed tomography, Eur. J. Radiol. 122 (2020), 108666, https://doi.org/10.1016/j.ejrad.2019.108666.

[11] M. Saeed, T.A. Van, R. Krug, S.W. Hetts, MaW. Wilson, Cardiac MR imaging: current status and future direction, Cardiovasc. Diagn. Ther. (2015) 290–310.

[12] C. Hamilton-Craig, D. Stäeb, A. al Najjar, K. O'Brien, W. Crawford, S. Fletcher, M. Barth, G. Galloway, 7-tesla functional cardiovascular mr using vectorcardiographic triggering—overcoming the magnetohydrodynamic effect, Tomography 7 (2021) 323–332, https://doi.org/10.3390/tomography7030029.

[13] J.W. Krug, G. Rose, G.D. Clifford, J. Oster, ECG-Based Gating in Ultra High Field Cardiovascular Magnetic Resonance Using an Independent Component Analysis Approach, 2013. http://jcmr-online.com/content/15/104http://jcmr-online.com/content/15/104.

[14] C.M. Kramer, J. Barkhausen, C. Bucciarelli-Ducci, S.D. Flamm, R.J. Kim, E. Nagel, Standardized cardiovascular magnetic resonance imaging (CMR) protocols: 2020 update, J. Cardiovasc. Magn. Reson. 22 (2020), https://doi.org/10.1186/s12968-020-00607-1.

[15] A. Esposito, M. Francone, R. Faletti, M. Centonze, F. Cademartiri, I. Carbone, R. de Rosa, E. di Cesare, L. la Grutta, G. Ligabue, L. Lovato, E. Maffei, R. Marano, M. Midiri, G. Pontone, L. Natale, F. de Cobelli, Lights and shadows of cardiac magnetic resonance imaging in acute myocarditis, Insights Imaging 7 (2016) 99–110, https://doi.org/10.1007/s13244-015-0444-7.

[16] P. Kellman, M.S. Hansen, T1-mapping in the heart: accuracy and precision, J. Cardiovasc. Magn. Reson. 16 (2014), https://doi.org/10.1186/1532-429X-16-2.

[17] S.K. Piechnik, V.M. Ferreira, E. Dall'Armellina, L.E. Cochlin, A. Greiser, S. Neubauer, M.D. Robson, Shortened Modified Look-Locker Inversion recovery (ShMOLLI) for clinical myocardial T1-mapping at 1.5 and 3 T within a 9 heartbeat breathhold, J. Cardiovasc. Magn. Reson. 12 (2010), https://doi.org/10.1186/1532-429X-12-69.

[18] S.M.O. Rauhalammi, K. Mangion, P.H. Barrientos, D.J.A. Carrick, G. Clerfond, J. McClure, C. McComb, A. Radjenovic, C. Berry, Native myocardial longitudinal (T1) relaxation time: regional, age, and sex associations in the healthy adult heart, J. Magn. Reson. Imag. 44 (2016) 541–548, https://doi.org/10.1002/jmri.25217.

[19] M. van de Giessen, Q. Tao, R.J. van der Geest, B.P.F. Lelieveldt, Model-based alignment of Look-Locker MRI sequences for calibrated myocardical scar tissue quantification, in: 2013 IEEE 10th International Symposium on Biomedical Imaging, San Francisco, CA, USA, 2013, pp. 1038–1041, https://doi.org/10.1109/ISBI.2013.6556655.

[20] A. Martinez-Naharro, A.J. Baksi, P.N. Hawkins, M. Fontana, Diagnostic imaging of cardiac amyloidosis, Nat. Rev. Cardiol. 17 (2020) 413–426, https://doi.org/10.1038/s41569-020-0334-7.

[21] N. Kawel-Boehm, S.J. Hetzel, B. Ambale-Venkatesh, G. Captur, C.J. Francois, M. Jerosch-Herold, M. Salerno, S.D. Teague, E. Valsangiacomo-Buechel, R.J. van der Geest, D.A. Bluemke, Reference ranges ("normal values") for cardiovascular magnetic resonance (CMR) in adults and children: 2020 update, J. Cardiovasc. Magn. Reson. 22 (2020), https://doi.org/10.1186/s12968-020-00683-3.

[22] M.L. Chuang, P. Gona, G.L.T.F. Hautvast, C.J. Salton, S.J. Blease, S.B. Yeon, M. Breeuwer, C.J. O, W.J. Manning, Correlation of Trabeculae and Papillary Muscles with Clinical and Cardiac Characteristics and Impact on CMR Measures of LV Anatomy and Function, 2012.

[23] J. Vogel-Claussen, J.P. Finn, A.S. Gomes, G.W. Hundley, M. Jerosch-Herold, G. Pearson, S. Sinha, J.A.C. Lima, D.A. Bluemke, Left Ventricular Papillary Muscle Mass: Relationship to Left Ventricular Mass and Volumes by Magnetic Resonance Imaging MRI and Equipment, 2006.

[24] J.H. Riffel, K. Schmucker, F. Andre, M. Ochs, K. Hirschberg, E. Schaub, T. Fritz, M. Mueller-Hennessen, E. Giannitsis, H.A. Katus, M.G. Friedrich, Cardiovascular magnetic resonance of cardiac morphology and function: impact of different strategies of contour drawing and indexing, Clin. Res. Cardiol. 108 (2019) 411–429, https://doi.org/10.1007/s00392-018-1371-7.

[25] G. Muscogiuri, V. Volpato, R. Cau, M. Chiesa, L. Saba, M. Guglielmo, A. Senatieri, G. Chierchia, G. Pontone, S. Dell'Aversana, U.J. Schoepf, M.G. Andrews, P. Basile, A.I. Guaricci, P. Marra, D. Muraru, L.P. Badano, S. Sironi, Application of AI in cardiovascular multimodality imaging, Heliyon 8 (2022), https://doi.org/10.1016/j.heliyon.2022.e10872.

[26] J.B. Geske, S.R. Ommen, B.J. Gersh, Hypertrophic cardiomyopathy: clinical update, JACC Heart Fail 6 (2018) 364–375, https://doi.org/10.1016/j.jchf.2018.02.010.

[27] M. de O. Antunes, T.L. Scudeler, Hypertrophic cardiomyopathy, IJC Heart and Vasculature 27 (2020), https://doi.org/10.1016/j.ijcha.2020.100503.

[28] M. Fogante, G. Agliata, M.C. Basile, P. Compagnucci, G. Volpato, U. Falanga, G. Stronati, F. Guerra, D. Vignale, A. Esposito, A. dello Russo, M. Casella, A. Giovagnoni, Cardiac imaging in athlete's heart: the role of the radiologist, Medicina (Lithuania) 57 (2021), https://doi.org/10.3390/medicina57050455.

[29] J.L. Zamorano, A. Anastasakis, M.A. Borger, M. Borggrefe, F. Cecchi, P. Charron, A.A. Hagege, A. Lafont, G. Limongelli, H. Mahrholdt, W.J. McKenna, J. Mogensen, P. Nihoyannopoulos, S. Nistri, P.G. Piepe, B. Pieske, C. Rapezzi, F.H. Rutten, C. Tillmanns, H. Watkins, C. O'Mahony, S. Achenbach, H. Baumgartner, J.J. Bax, H. Bueno, V. Dean, C. Deaton, Ç. Erol, R. Fagard, R. Ferrari, D. Hasdai, A.W. Hoes, P. Kirchhof, J. Knuuti, P. Kolh, P. Lancellotti, A. Linhart, M.F. Piepoli, P. Ponikowski, P.A. Sirnes, J.L. Tamargo, M. Tendera, A. Torbicki, W. Wijns, S. Windecker, F. Alfonso, C. Basso, N.M. Cardim, J. R. Gimeno, S. Heymans, P.J. Holm, A. Keren, C. Lionis, C. Muneretto, S. Priori, M.J. Salvador, C. Wolpert, 2014 ESC guidelines on diagnosis and management of hypertrophic cardiomyopathy: the task force for the diagnosis and management of hypertrophic cardiomyopathy of the European Society of Cardiology (ESC), Eur. Heart J. 35 (2014) 2733–2779, https://doi.org/10.1093/eurheartj/ehu284.

[30] N. Hensley, J. Dietrich, D. Nyhan, N. Mitter, M.S. Yee, M.B. Brady, Hypertrophic cardiomyopathy: a review, Anesth. Analg. 120 (2015) 554–569, https://doi.org/10.1213/ANE.0000000000000538.

[31] L.C. Poliac, M.E. Barron, B.J. Maron, Hypertrophic Cardiomyopathy, 2006. http://www.hpcgg.org;.

[32] P.G. Camici, I. Olivotto, O.E. Rimoldi, The coronary circulation and blood flow in left ventricular hypertrophy, J. Mol. Cell. Cardiol. 52 (2012) 857–864, https://doi.org/10.1016/j.yjmcc.2011.08.028.

[33] M. Gatti, A. Carisio, T. D'Angelo, F. Darvizeh, S. Dell'Aversana, D. Tore, M. Centonze, R. Faletti, Cardiovascular magnetic resonance in myocardial infarction with non-obstructive coronary arteries patients: a review, World J. Cardiol. 12 (2020) 248–261, https://doi.org/10.4330/wjc.v12.i6.248.

[34] A. Rudolph, H. Abdel-Aty, S. Bohl, P. Boyé, A. Zagrosek, R. Dietz, J. Schulz-Menger, Noninvasive detection of fibrosis applying contrast-enhanced cardiac magnetic resonance in different forms of left ventricular hypertrophy. Relation to remodeling, J. Am. Coll. Cardiol. 53 (2009) 284–291, https://doi.org/10.1016/j.jacc.2008.08.064.

[35] R.H. Chan, B.J. Maron, I. Olivotto, M.J. Pencina, G.E. Assenza, T. Haas, J.R. Lesser, C. Gruner, A.M. Crean, H. Rakowski, J.E. Udelson, E. Rowin, M. Lombardi, F. Cecchi, B. Tomberli, P. Spirito, F. Formisano, E. Biagini, C. Rapezzi, C.N. de Cecco, C. Autore, E.F. Cook, S.N. Hong, C.M. Gibson, W.J. Manning,

E. Appelbaum, M.S. Maron, Prognostic value of quantitative contrast-enhanced cardiovascular magnetic resonance for the evaluation of sudden death risk in patients with hypertrophic cardiomyopathy, Circulation 130 (2014) 484–495, https://doi.org/10.1161/CIRCULATIONAHA.113.007094.
[36] M.S. Maron, J.J. Finley, J.M. Bos, T.H. Hauser, W.J. Manning, T.S. Haas, J.R. Lesser, J.E. Udelson, M.J. Ackerman, B.J. Maron, Prevalence, clinical significance, and natural history of left ventricular apical aneurysms in hypertrophic cardiomyopathy, Circulation 118 (2008) 1541–1549, https://doi.org/10.1161/CIRCULATIONAHA.108.781401.
[37] M. Gatti, T. D'Angelo, G. Muscogiuri, S. Dell'aversana, A. Andreis, A. Carisio, F. Darvizeh, D. Tore, G. Pontone, R. Faletti, Cardiovascular magnetic resonance of cardiac tumors and masses, World J. Cardiol. 13 (2021) 628–649, https://doi.org/10.4330/WJC.V13.I11.628.
[38] C. Bakogiannis, D. Mouselimis, A. Tsarouchas, E. Papatheodorou, V.P. Vassilikos, E. Androulakis, Hypertrophic cardiomyopathy or athlete's heart? A systematic review of novel cardiovascular magnetic resonance imaging parameters, Eur. J. Sport Sci. (2021) 1–12, https://doi.org/10.1080/17461391.2021.2001576.
[39] M. Galderisi, N. Cardim, A. D'Andrea, O. Bruder, B. Cosyns, L. Davin, E. Donal, T. Edvardsen, A. Freitas, G. Habib, A. Kitsiou, S. Plein, S.E. Petersen, B. A. Popescu, S. Schroeder, C. Burgstahler, P. Lancellotti, Themulti-modality cardiac imaging approach to the Athletés heart: an expert consensus of the European Association of Cardiovascular Imaging, Eur Heart J Cardiovasc Imaging 16 (2015), https://doi.org/10.1093/ehjci/jeu323, 353T-353.
[40] C. de Innocentiis, F. Ricci, M.Y. Khanji, N. Aung, C. Tana, E. Verrengia, S.E. Petersen, S. Gallina, Athlete's heart: diagnostic challenges and future perspectives, Sports Med. 48 (2018) 2463–2477, https://doi.org/10.1007/s40279-018-0985-2.
[41] A. Martinez-Naharro, T. Kotecha, K. Norrington, M. Boldrini, T. Rezk, C. Quarta, T.A. Treibel, C.J. Whelan, D.S. Knight, P. Kellman, F.L. Ruberg, J.D. Gillmore, J. C. Moon, P.N. Hawkins, M. Fontana, Native T1 and extracellular volume in transthyretin amyloidosis, JACC Cardiovasc Imaging 12 (2019) 810–819, https://doi.org/10.1016/j.jcmg.2018.02.006.
[42] A.M. Maceira, J. Joshi, S.K. Prasad, J.C. Moon, E. Perugini, I. Harding, M.N. Sheppard, P.A. Poole-Wilson, P.N. Hawkins, D.J. Pennell, Cardiovascular magnetic resonance in cardiac amyloidosis, Circulation 111 (2005) 186–193, https://doi.org/10.1161/01.CIR.0000152819.97857.9D.
[43] G. Palladini, P. Milani, G. Merlini, Management of AL amyloidosis in 2020, Blood 136 (23) (2020) 2620–2627, https://doi.org/10.1182/blood.2020006913.
[44] M. Fontana, S.M. Banypersad, T.A. Treibel, A. Abdel-Gadir, V. Maestrini, T. Lane, J.A. Gilbertson, D.F. Hutt, H.J. Lachmann, C.J. Whelan, A.D. Wechalekar, A. S. Herrey, J.D. Gillmore, P.N. Hawkins, J.C. Moon, Differential myocyte responses in patients with cardiac transthyretin amyloidosis and light-chain amyloidosis: a cardiac MR imaging study, Radiology 277 (2015) 388–397, https://doi.org/10.1148/radiol.2015141744.
[45] J.L. Cavalcante, S. Rijal, I. Abdelkarim, A.D. Althouse, M.S. Sharbaugh, Y. Fridman, P. Soman, D.E. Forman, J.T. Schindler, T.G. Gleason, J.S. Lee, E.B. Schelbert, Cardiac amyloidosis is prevalent in older patients with aortic stenosis and carries worse prognosis, J. Cardiovasc. Magn. Reson. 19 (2017) 98, https://doi.org/10.1186/s12968-017-0415-x.
[46] T.A. Treibel, M. Fontana, J.A. Gilbertson, S. Castelletti, S.K. White, P.R. Scully, N. Roberts, D.F. Hutt, D.M. Rowczenio, C.J. Whelan, M.A. Ashworth, J. D. Gillmore, P.N. Hawkins, J.C. Moon, Occult transthyretin cardiac amyloid in severe calcific aortic stenosis, Circ Cardiovasc Imaging 9 (2016), https://doi.org/10.1161/CIRCIMAGING.116.005066.
[47] P.R. Scully, T.A. Treibel, M. Fontana, G. Lloyd, M. Mullen, F. Pugliese, N. Hartman, P.N. Hawkins, L.J. Menezes, J.C. Moon, Prevalence of cardiac amyloidosis in patients referred for transcatheter aortic valve replacement, J. Am. Coll. Cardiol. 71 (2018) 463–464, https://doi.org/10.1016/j.jacc.2017.11.037.
[48] P.R. Scully, K.P. Patel, B. Saberwal, E. Klotz, J.B. Augusto, G.D. Thornton, R.K. Hughes, C. Manisty, G. Lloyd, J.D. Newton, N. Sabharwal, A. Kelion, S. Kennon, M. Ozkor, M. Mullen, N. Hartman, J.L. Cavalcante, L.J. Menezes, P.N. Hawkins, T.A. Treibel, J.C. Moon, F. Pugliese, Identifying cardiac amyloid in aortic stenosis: ECV quantification by CT in TAVR patients, JACC Cardiovasc Imaging 13 (2020) 2177–2189, https://doi.org/10.1016/j.jcmg.2020.05.029.
[49] J.L. Tan, H.K. Fong, E.Y. Birati, Y. Han, Cardiac sarcoidosis, Am. J. Cardiol. 123 (2019) 513–522, https://doi.org/10.1016/j.amjcard.2018.10.021.
[50] S. Silvera, K. Strach, J. Bogaert, T. Sommer, O. Vignaux, Cardiomyopathies (hypertrophy and failure): what can offer cardiac magnetic resonance imaging? Presse Med. 40 (2011) https://doi.org/10.1016/j.lpm.2010.12.016.
[51] E. Markatis, A. Afthinos, E. Antonakis, I.C. Papanikolaou, Cardiac sarcoidosis: diagnosis and management, Rev. Cardiovasc. Med. 21 (2020) 321–338, https://doi.org/10.31083/j.rcm.2020.03.102.
[52] E. Hulten, V. Agarwal, M. Cahill, G. Cole, T. Vita, S. Parrish, M.S. Bittencourt, V.L. Murthy, R. Kwong, M.F. di Carli, R. Blankstein, Presence of late gadolinium enhancement by cardiac magnetic resonance among patients with suspected cardiac sarcoidosis is associated with adverse cardiovascular prognosis: a systematic review and meta-analysis, Circ Cardiovasc Imaging 9 (2016), https://doi.org/10.1161/CIRCIMAGING.116.005001.
[53] P. Mankad, B. Mitchell, D. Birnie, J. Kron, Cardiac sarcoidosis, Curr. Cardiol. Rep. 21 (2019) 152, https://doi.org/10.1007/s11886-019-1238-1.
[54] S. Greulich, D. Kitterer, J. Latus, E. Aguor, H. Steubing, P. Kaesemann, A. Patrascu, A. Greiser, S. Groeninger, A. Mayr, N. Braun, M.D. Alscher, U. Sechtem, H. Mahrholdt, Comprehensive cardiovascular magnetic resonance assessment in patients with sarcoidosis and preserved left ventricular ejection fraction, Circ Cardiovasc Imaging 9 (2016), https://doi.org/10.1161/CIRCIMAGING.116.005022.
[55] E. Crouser, C. Ono, T. Tran, X. He, S. Raman, Improved Detection of Cardiac SarcoidosisUsing Magnetic Resonance with MyocardialT2 Mapping, 2014, https://doi.org/10.1164/rccm.201309-1668LE.
[56] E.C. Wicks, L.J. Menezes, A. Barnes, S.A. Mohiddin, N. Sekhri, J.C. Porter, H.L. Booth, E. Garrett, R.S. Patel, M. Pavlou, A.M. Groves, P.M. E lliott, Diagnostic accuracy and prognostic value of simultaneous hybrid 18 F-fluorodeoxyglucose positron emission tomography/magnetic resonance imaging in cardiac sarcoidosis, Eur Heart J Cardiovasc Imaging 19 (2018) 757–767, https://doi.org/10.1093/ehjci/jex340.
[57] O. Manabe, N. Oyama-Manabe, T. Aikawa, S. Tsuneta, N. Tamaki, Advances in diagnostic imaging for cardiac sarcoidosis, J. Clin. Med. 10 (2021), https://doi.org/10.3390/jcm10245808.
[58] N.L. Pereira, M. Grogan, G.W. Dec, Spectrum of restrictive and infiltrative cardiomyopathies: Part 1 of a 2-Part Series, J. Am. Coll. Cardiol. 71 (2018) 1130–1148, https://doi.org/10.1016/j.jacc.2018.01.016.
[59] N. Galea, G. Polizzi, M. Gatti, G. Cundari, M. Figuera, R. Faletti, Cardiovascular magnetic resonance (CMR) in restrictive cardiomyopathies, Radiologia Medica 125 (2020) 1072–1086, https://doi.org/10.1007/s11547-020-01287-8.
[60] C. Kampmann, F. Baehner, C. Whybra, C. Martin, C.M. Wiethoff, M. Ries, A. Gal, M. Beck, Cardiac Manifestations of Anderson-Fabry Disease in Heterozygous Females, 2002.
[61] R. Perry, R. Shah, M. Saiedi, S. Patil, A. Ganesan, A. Linhart, J.B. Selvanayagam, The role of cardiac imaging in the diagnosis and management of anderson-fabry disease, JACC Cardiovasc Imaging 12 (2019) 1230–1242, https://doi.org/10.1016/j.jcmg.2018.11.039.
[62] T. Kubo, H. Kitaoka, Imaging of left ventricular hypertrophy: a practical utility for differential diagnosis and assessment of disease severity, Curr. Cardiol. Rep. 19 (2017), https://doi.org/10.1007/s11886-017-0875-5.
[63] M. Pieroni, J.C. Moon, E. Arbustini, R. Barriales-Villa, A. Camporeale, A.C. Vujkovac, P.M. Elliott, A. Hagege, J. Kuusisto, A. Linhart, P. Nordbeck, I. Olivotto, P. Pietilä-Effati, M. Namdar, Cardiac involvement in fabry disease: JACC review topic of the week, J. Am. Coll. Cardiol. 77 (2021) 922–936, https://doi.org/10.1016/j.jacc.2020.12.024.
[64] J.C. Wu, C.Y. Ho, H. Skali, R. Abichandani, W.R. Wilcox, M. Banikazemi, S. Packman, K. Sims, S.D. Solomon, Cardiovascular manifestations of fabry disease: relationships between left ventricular hypertrophy, disease severity, and-galactosidase a activity, Eur. Heart J. 31 (2010) 1088–1097, https://doi.org/10.1093/eurheartj/ehp588.
[65] S. Nordin, R. Kozor, K. Medina-Menacho, A. Abdel-Gadir, S. Baig, D.M. Sado, I. Lobascio, E. Murphy, R.H. Lachmann, A. Mehta, N.C. Edwards, U. Ramaswami, R.P. Steeds, D. Hughes, J.C. Moon, Proposed stages of myocardial phenotype development in fabry disease, JACC Cardiovasc Imaging 12 (2019) 1673–1683, https://doi.org/10.1016/j.jcmg.2018.03.020.
[66] C. Izgi, V. Vassiliou, A.J. Baksi, S.K. Prasad, Differential diagnosis of left ventricular hypertrophy: usefulness of multimodality imaging and tissue characterization with cardiac magnetic resonance, Echocardiography 33 (2016) 1765–1768, https://doi.org/10.1111/echo.13367.
[67] D.M. Sado, S.K. White, S.K. Piechnik, S.M. Banypersad, T. Treibel, G. Captur, M. Fontana, V. Maestrini, A.S. Flett, M.D. Robson, R.H. Lachmann, E. Murphy, A. Mehta, D. Hughes, S. Neubauer, P.M. Elliott, J.C. Moon, Identification and assessment of anderson-fabry disease by cardiovascular magnetic resonance noncontrast myocardial T1 mapping, Circ Cardiovasc Imaging 6 (2013) 392–398, https://doi.org/10.1161/CIRCIMAGING.112.000070.
[68] S. Pica, D.M. Sado, V. Maestrini, M. Fontana, S.K. White, T. Treibel, G. Captur, S. Anderson, S.K. Piechnik, M.D. Robson, R.H. Lachmann, E. Murphy, A. Mehta, D. Hughes, P. Kellman, P.M. Elliott, A.S. Herrey, J.C. Moon, Reproducibility of native myocardial T1 mapping in the assessment of Fabry disease and its role in

early detection of cardiac involvement by cardiovascular magnetic resonance, J. Cardiovasc. Magn. Reson. 16 (2014) 99, https://doi.org/10.1186/s12968-014-0099-4.
[69] A. Frustaci, R. Verardo, C. Grande, N. Galea, P. Piselli, I. Carbone, M. Alfarano, M.A. Russo, C. Chimenti, Immune-mediated myocarditis in fabry disease cardiomyopathy, J. Am. Heart Assoc. 7 (2018), https://doi.org/10.1161/JAHA.118.009052.
[70] H. Hazari, I. Belenkie, A. Kryski, J.A. White, G.Y. Oudit, R. Thompson, T. Fung, N. Dehar, A. Khan, Comparison of cardiac magnetic resonance imaging and echocardiography in assessment of left ventricular hypertrophy in fabry disease, Can. J. Cardiol. 34 (2018) 1041–1047, https://doi.org/10.1016/j.cjca.2018.03.011.
[71] M. Arends, M. Biegstraaten, D.A. Hughes, A. Mehta, P.M. Elliott, D. Oder, O.T. Watkinson, F.M. Vaz, A.B.P. van Kuilenburg, C. Wanner, C.E.M. Hollak, Retrospective study of long-term outcomes of enzyme replacement therapy in Fabry disease: analysis of prognostic factors, PLoS One 12 (2017), https://doi.org/10.1371/journal.pone.0182379.
[72] M. Motwani, S. Banypersad, P. Woolfson, S. Waldek, Enzyme replacement therapy improves cardiac features and severity of Fabry disease, Mol. Genet. Metabol. 107 (2012) 197–202, https://doi.org/10.1016/j.ymgme.2012.05.011.
[73] S. Nordin, R. Kozor, R. Vijapurapu, J.B. Augusto, K.D. Knott, G. Captur, T.A. Treibel, U. Ramaswami, M. Tchan, T. Geberhiwot, R.P. Steeds, D.A. Hughes, J. C. Moon, Myocardial storage, inflammation, and cardiac phenotype in fabry disease after one year of enzyme replacement therapy, Circ Cardiovasc Imaging 12 (2019), https://doi.org/10.1161/CIRCIMAGING.119.009430.
[74] V. Nair, E.C. Belanger, J.P. Veinot, Lysosomal storage disorders affecting the heart: a review, Cardiovasc. Pathol. 39 (2019) 12–24, https://doi.org/10.1016/j.carpath.2018.11.002.
[75] F.M. Platt, A. d'Azzo, B.L. Davidson, E.F. Neufeld, C.J. Tifft, Lysosomal storage diseases, Nat. Rev. Dis. Prim. 4 (2018) 27, https://doi.org/10.1038/s41572-018-0025-4.
[76] M. Boentert, A. Florian, B. Dräger, P. Young, A. Yilmaz, Pattern and prognostic value of cardiac involvement in patients with late-onset pompe disease: a comprehensive cardiovascular magnetic resonance approach, J. Cardiovasc. Magn. Reson. 18 (2016), https://doi.org/10.1186/s12968-016-0311-9.
[77] P.C.A. Barker, S.K. Pasquali, S. Darty, R.J. Ing, J.S. Li, R.J. Kim, S. DeArmey, P.S. Kishnani, M.J. Campbell, Use of cardiac magnetic resonance imaging to evaluate cardiac structure, function and fibrosis in children with infantile Pompe disease on enzyme replacement therapy, Mol. Genet. Metabol. 101 (2010) 332–337, https://doi.org/10.1016/j.ymgme.2010.07.011.
[78] A. Miliou, A.S. Antonopoulos, N. Kouris, G. Lazaros, K. Tsioufis, C. Vlachopoulos, Danon cardiomyopathy: specific imaging signs, JACC Case Rep 4 (2022) 1496–1500, https://doi.org/10.1016/j.jaccas.2022.08.007.
[79] N.R. Shah, A.S. Eisman, D.E. Winchester, A.R. Morrison, R. Qureshi, I.N. Sarkar, W.C. Wu, E-consult protocoling to improve the quality of cardiac stress tests, JACC Cardiovasc Imaging 14 (2021) 512–514, https://doi.org/10.1016/j.jcmg.2020.08.009.
[80] G. Nucifora, D. Miani, G. Piccoli, A. Proclemer, Cardiac magnetic resonance imaging in Danon disease, Cardiology 121 (2012) 27–30, https://doi.org/10.1159/000336448.
[81] E.A. Braunlin, P.R. Harmatz, M. Scarpa, B. Furlanetto, C. Kampmann, J.P. Loehr, K.P. Ponder, W.C. Roberts, H.M. Rosenfeld, R. Giugliani, Cardiac disease in patients with mucopolysaccharidosis: presentation, diagnosis and management, J. Inherit. Metab. Dis. 34 (2011) 1183–1197, https://doi.org/10.1007/s10545-011-9359-8.
[82] M. Mostefa Kara, P. de Groote, G. Abboud, I. Tillie-Leblond, F. Mouquet, Cardiac magnetic resonance imaging of mucopolysaccharidosis type II cardiomyopathy, Int. J. Cardiol. 147 (2011) 170–171, https://doi.org/10.1016/j.ijcard.2010.10.089.
[83] C.C. Hsu, N.H. Senussi, K.Y. Fertrin, K.v. Kowdley, Iron overload disorders, Hepatol Commun 6 (2022) 1842–1854, https://doi.org/10.1002/hep4.2012.
[84] D. Girelli, F. Busti, P. Brissot, I. Cabantchik, M.U. Muckenthaler, G. Porto, Hemochromatosis Classification: Update and Recommendations by the, BIOIRON Society, 2022.
[85] A.T. Taher, A.N. Saliba, EMERGING ISSUES IN CLINICAL CARE IN THALASSEMIA | Iron Overload in Thalassemia: Different Organs at Different Rates, 2017, https://doi.org/10.1182/asheducation-2017.1.265.
[86] P. Gujja, D.R. Rosing, D.J. Tripodi, Y. Shizukuda, Iron overload cardiomyopathy: better understanding of an increasing disorder, J. Am. Coll. Cardiol. 56 (2010) 1001–1012, https://doi.org/10.1016/j.jacc.2010.03.083.
[87] P. Triadyaksa, M. Oudkerk, P.E. Sijens, Cardiac T2* mapping: techniques and clinical applications, J. Magn. Reson. Imag. 52 (2020) 1340–1351, https://doi.org/10.1002/jmri.27023.
[88] V. Ferrari, The EACVI Textbook of Cardiovascular Magnetic Resonance, Oxford University Press, 2018, https://doi.org/10.1093/med/9780198779735.001.0001.
[89] N. Rezaeian, M.A. Mohtasham, A.J. Khaleel, N. Parnianfard, K. Kasani, R. Golshan, Comparison of global strain values of myocardium in beta-thalassemia major patients with iron load using specific feature tracking in cardiac magnetic resonance imaging, Int. J. Cardiovasc. Imag. 36 (2020) 1343–1349, https://doi.org/10.1007/s10554-020-01835-3.
[90] E. Tahir, R. Fischer, R. Grosse, P. Tavrovski, J. Yamamura, J. Starekova, G.K. Lund, P. Bannas, J. Graessner, U.K. Radunski, K. Muellerleile, G. Adam, B. P. Schoennagel, Strain analysis using feature-tracking CMR to detect LV systolic dysfunction in myocardial iron overload disease, JACC Cardiovasc Imaging 13 (2020) 2267–2268, https://doi.org/10.1016/j.jcmg.2020.05.026.
[91] V. Ojha, K.P. Ganga, T. Seth, A. Roy, N. Naik, P. Jagia, G.S. Gulati, S. Kumar, S. Sharma, Role of CMR feature-tracking derived left ventricular strain in predicting myocardial iron overload and assessing myocardial contractile dysfunction in patients with thalassemia major, Eur. Radiol. 31 (2021) 6184–6192, https://doi.org/10.1007/s00330-020-07599-7.